



# Vertically stacked microscale organic nonvolatile memory devices toward three-dimensional high integration



Daekyoung Yoo<sup>a</sup>, Younggul Song<sup>a</sup>, Jingon Jang<sup>a</sup>, Wang-Taek Hwang<sup>a</sup>, Seok-Heon Jung<sup>b</sup>,  
Seunghun Hong<sup>a</sup>, Jin-Kyun Lee<sup>b</sup>, Takhee Lee<sup>a,\*</sup>

<sup>a</sup> Department of Physics and Astronomy, and Institute of Applied Physics, Seoul National University, Seoul 151-747, South Korea

<sup>b</sup> Department of Polymer Science and Engineering, Inha University, Incheon 402-751, South Korea

## ARTICLE INFO

### Article history:

Received 10 December 2014

Received in revised form 10 March 2015

Accepted 15 March 2015

Available online 16 March 2015

### Keywords:

Organic memory

Nonvolatile memory

Vertical stack

Microscale organic devices

Three-dimensional integration

## ABSTRACT

In this study, vertically stacked microscale organic resistive nonvolatile memory devices are demonstrated. The fabricated devices consisted of vertically stacked two layers of  $32 \times 32$  crossbar-structured organic memory devices (total of 2048 memory cells) with a memory-cell size of  $7 \times 7 \mu\text{m}^2$  on a  $\text{SiO}_2$  substrate. The microscale organic memory devices were made using an orthogonal photolithography technique with a highly fluorinated photoresist and development solvent. The vertically stacked microscale organic memory devices showed reproducibility with good endurance, and stability and long retention times (over  $10^4$  s) for both layers. The realization of vertical stacking of microscale organic memory devices might enable the production of organic memory devices toward the three-dimensional integration of organic electronic devices.

© 2015 Elsevier B.V. All rights reserved.

## 1. Introduction

Organic electronic devices have great potentials due to their low-cost fabrication with attributes such as solution process, printability, roll-to-roll fabrication, organic material variety, and flexibility [1–7]. Numerous studies have reported on organic electronic devices, such as organic field-effect transistors, light-emitting diodes, solar cells, and nonvolatile memory devices [8–16]. In particular, organic nonvolatile memory has been spotlighted for data-storage applications because of the quality and characteristics described above [17–19]. However, despite these merits, most organic memory devices have been fabricated in very low densities and with large memory-cell sizes, typically hundreds of microns. The reason for this limitation is that the standard chemicals and solvents for conventional photolithography that are necessary to produce microscale patterns damage the existing organic layers during the photolithographic development and lift-off process. To overcome this problem, a chemically nondestructive orthogonal photolithographic method has been developed [20]. Orthogonality is a property that is required to protect the underlying organic layers from the addition of lithographic chemicals and allow the removal of the unnecessary part of the deposited photoresist layer by the developing solvents. For example, highly

fluorinated chemicals and fluorosolvents are orthogonal to most organic materials and do not damage the underlying organic layers during the photolithographic processes [21]. We have recently applied orthogonal photolithography and demonstrated flexible microscale organic field-effect transistors [22,23] and microscale organic memory devices [24]. In particular, orthogonal photolithography has enabled microscale organic memory devices with much higher memory cell densities ( $64 \times 64$  single layer array with a  $10 \times 10 \mu\text{m}^2$  cell size) [24].

In addition to the microscale cell patterns, three-dimensional stacked integration can be an effective way to increase the device-cell density [25]. We have previously demonstrated vertical stacking of three layers of organic memory cells [26]. However, the individual organic memory-cell size in this study was  $200 \times 200 \mu\text{m}^2$  because a non-lithographic fabrication method involving shadow masks was employed to fabricate the organic memory devices [26]. Therefore, it would be worth investigating the possibility of combining orthogonal photolithography to produce microscale memory-cell patterns and three-dimensional vertical-stack integration to enhance the cell density of organic memory devices.

In this study, vertically stacked microscale organic memory devices using a composite of polyimide (PI) and 6-phenyl-C61 butyric acid methyl ester (PCBM) (purchased from Sigma Aldrich) are demonstrated. Specifically, vertically stacked double layers of  $32 \times 32$  crossbar-type PI:PCBM organic memory devices with a cell

\* Corresponding author.

E-mail address: [tlee@snu.ac.kr](mailto:tlee@snu.ac.kr) (T. Lee).

size of  $7 \times 7 \mu\text{m}^2$  were fabricated by orthogonal photolithography using fluorinated photoresist and solvents. The fabricated double-layer microscale organic memory devices exhibited typical resistive nonvolatile memory performance, such as a good ON/OFF ratio, stable switching characteristics, and good durability in terms of endurance and retention characteristics.

## 2. Experimental section

Fig. 1a shows the process schematics of the vertically stacked double layer microscale organic memory devices that were fabricated by orthogonal photolithography. Basically, we followed the fabrication processes that we previously reported [27]. First, a  $\text{SiO}_2$  (270 nm thick)/Si substrate was cleaned by ultrasonication using deionized (DI) water, acetone, and isopropanol (IPA) for 10 min at each step. Then, a 30 nm-thick Al layer was deposited on the substrate by a thermal evaporator with a deposition rate of  $0.5 \text{ \AA/s}$  at a pressure  $\sim 10^{-6}$  torr. The Al layer was patterned as a bottom electrode with a line width of  $7 \mu\text{m}$ , using conventional photolithography and the lift-off process. To enhance the surface uniformity of the Al electrode lines, they were exposed to UV-ozone for 10 min [27]. To prepare the organic memory active material, we used biphenyltetracarboxylic acid dianhydride p-phenylene diamine (BPDA-PPD):N-methyl-2pyrrolidone (NMP) (purchased from Sigma Aldrich) at a 1:9 weight ratio as a PI precursor, with 0.5 wt% PCBM in this solution. Next, 0.5 ml of PCBM solution and 2 ml of BPDA-PPD solution were mixed for the resistive active memory material (PI:PCBM) and then diluted with 11.5 ml of NMP to control the active-layer thickness. The PI:PCBM memory solution was spin-coated onto the Al electrode/substrate at 500 rpm for 5 s, followed by 1500 rpm for 30 s. Then, the coated film was soft-baked at  $120^\circ\text{C}$  for 8 min, followed by hard-baking at  $300^\circ\text{C}$  for 30 min on a hotplate in a  $\text{N}_2$ -filled glove box to dry and harden the deposited organic active layer [24,26,28]. Then, to fabricate the middle electrodes at the microscale, we employed orthogonal photolithography using semi-perfluoroalkyl resorcinarene (denoted as  $\text{R}_F$ -Calix-tBoc), a highly fluorinated chemical, as the photoresist and 3-ethoxy-1,1,1,2,3,4,4,5,5,6,6,6,-dodecafluoro-2trifluoromethylhexane (denoted as HFE-7200) as the developer. The chemical structures of  $\text{R}_F$ -Calix-tBoc and HFE-7200,

along with PI and PCBM, are provided in Fig. S1 of the supplementary material. The fluorinated photoresist solution was spin-coated onto the substrate at 1500 rpm for 50 s. Then, the coated fluorinated photoresist layer was exposed to UV radiation (416 nm wavelength, intensity of  $\sim 8 \text{ mW/cm}^2$ ) for 5–6 s through a photomask with  $7 \mu\text{m}$ -width line patterns (left picture of Fig. 1a). After baking at  $75^\circ\text{C}$  for 3 min, the photoresist layer was developed using HFE-7200 and dried with a  $\text{N}_2$  gas blower. Because the fluorinated photoresist is a negative photoresist, the UV-exposed regions of the photoresist layer lose their solubility in HFE-7200 during the development process, whereas unexposed regions are washed away by HFE-7200. This process enables the microscale patterning of intermediate electrodes without damaging the underlying PI:PCBM active memory layer (second left picture of Fig. 1a). Then, 30 nm-thick Al was deposited onto the samples using a thermal evaporator with a deposition rate of  $0.4 \text{ \AA/s}$  at a pressure of  $\sim 10^6$  torr. The unnecessary portion of the Al metal layer on the remaining photoresist layer was washed away using a lift-off solvent (HFE7200: EtOH = 10:1 weight ratio). During the lift-off process, only the Al layer directly deposited on the PI:PCBM memory layer can remain, which acts as the top electrode for the first PI:PCBM organic memory layer and the bottom electrode for the second PI:PCBM organic memory layer. To form the second PI:PCBM organic memory layer, we repeated the processes described above (second right and right pictures of Fig. 1a). The fabrication processes are described in greater detail in Fig. S2 of the supplementary material. Fig. 1b shows a schematic of the completed microscale organic memory devices that were fabricated as vertically stacked double layers, with each layer containing a  $32 \times 32$  crossbar-structure memory array (total of 2048 memory cells). Fig. 1c shows optical microscope images of the fabricated devices with a memory-cell size of  $7 \times 7 \mu\text{m}^2$ . These images suggest that the microscale Al electrodes were well developed and aligned. Note that vertically stackable microscale organic memory is the main idea in this study in comparison with our previous study result of single layer of microscale organic memory devices [24].

We examined the individual layers of the fabricated vertically stacked microscale organic memory devices. Fig. 2a shows the cross-sectional transmission electron microscope (TEM) image of the memory devices. The colored lines in Fig. 2a are energy

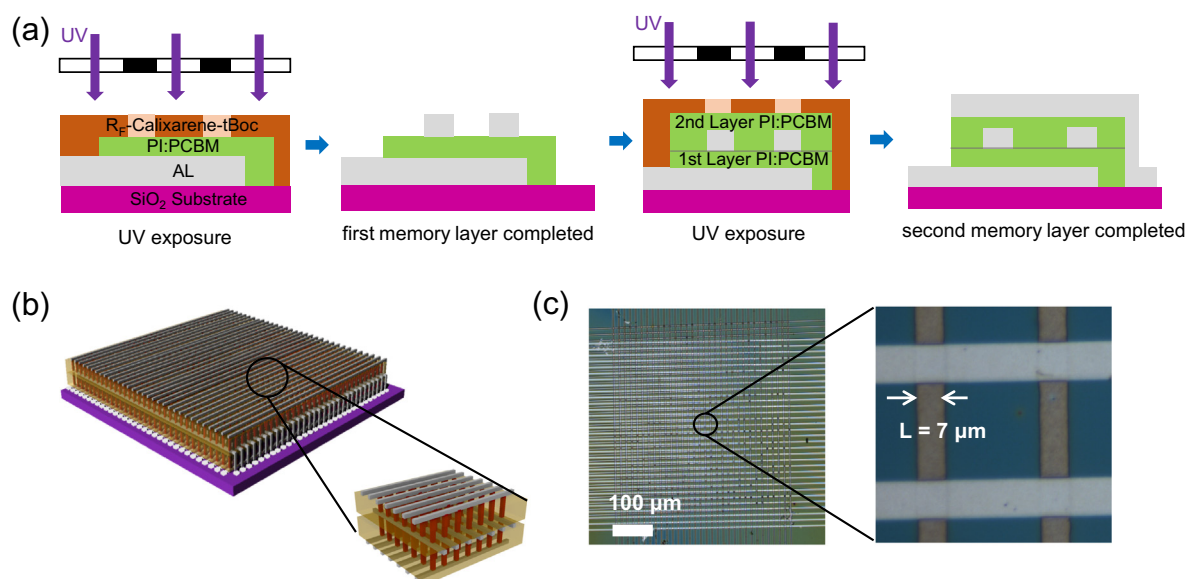
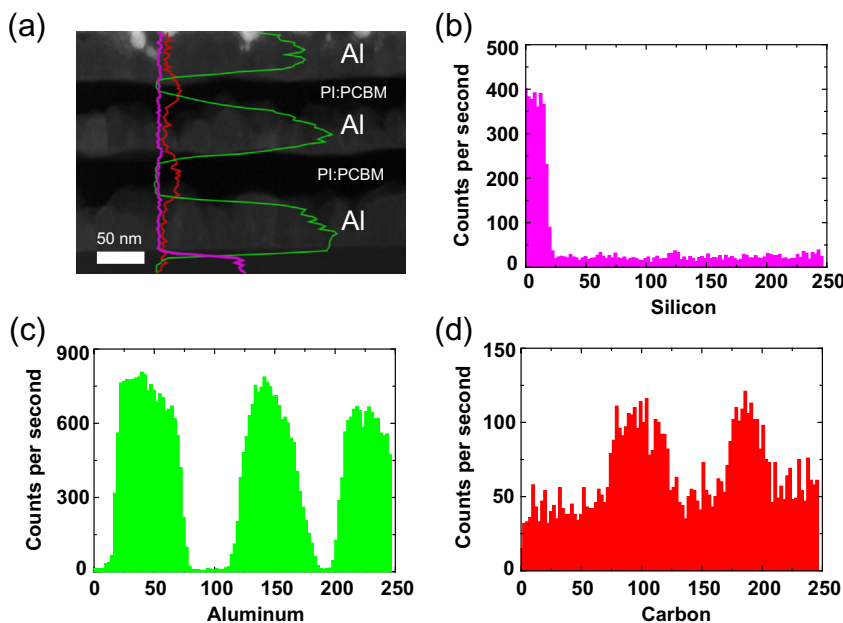


Fig. 1. (a) The fabrication process of vertically stacked double layers of microscale organic memory devices on a  $\text{SiO}_2$  substrate. (b) A schematic illustration of vertically stacked  $32 \times 32$  crossbar memory arrays. (c) Optical microscopic images of the fabricated microscale organic memory devices.



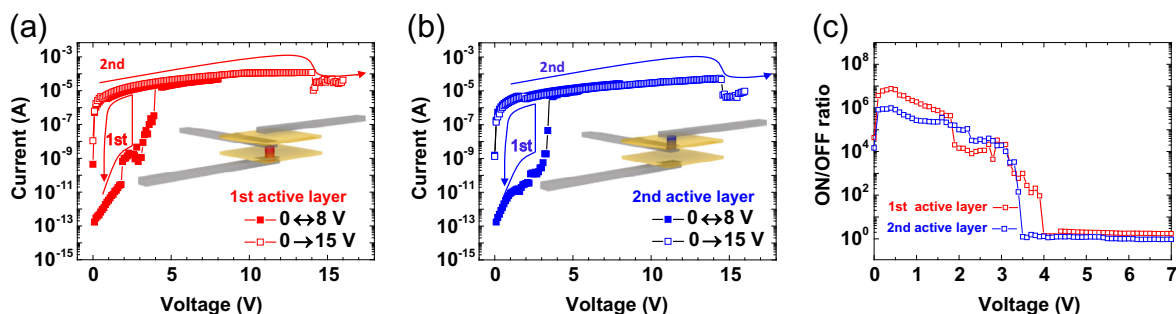
**Fig. 2.** (a) Cross-sectional TEM image of vertically stacked microscale organic memory devices. The device was sliced by a focused ion beam. (b–d) TEM EDS element profiles of the microscale organic memory devices. Each element profile exhibits a different color and peak according to the elements aluminum, carbon, and silicon contained in all layers. (For interpretation of the references to color in this figure legend, the reader is referred to the web version of this article.)

dispersive X-ray spectroscopy (EDS) measurement data (Fig. 2b–d), indicating that the unwanted penetration of Al was not observed in the organic memory layers. Carbon elements appeared high in counts per second for the two PI:PCBM organic memory layers, and the two active PI:PCBM layers were well separated (Fig. 2d).

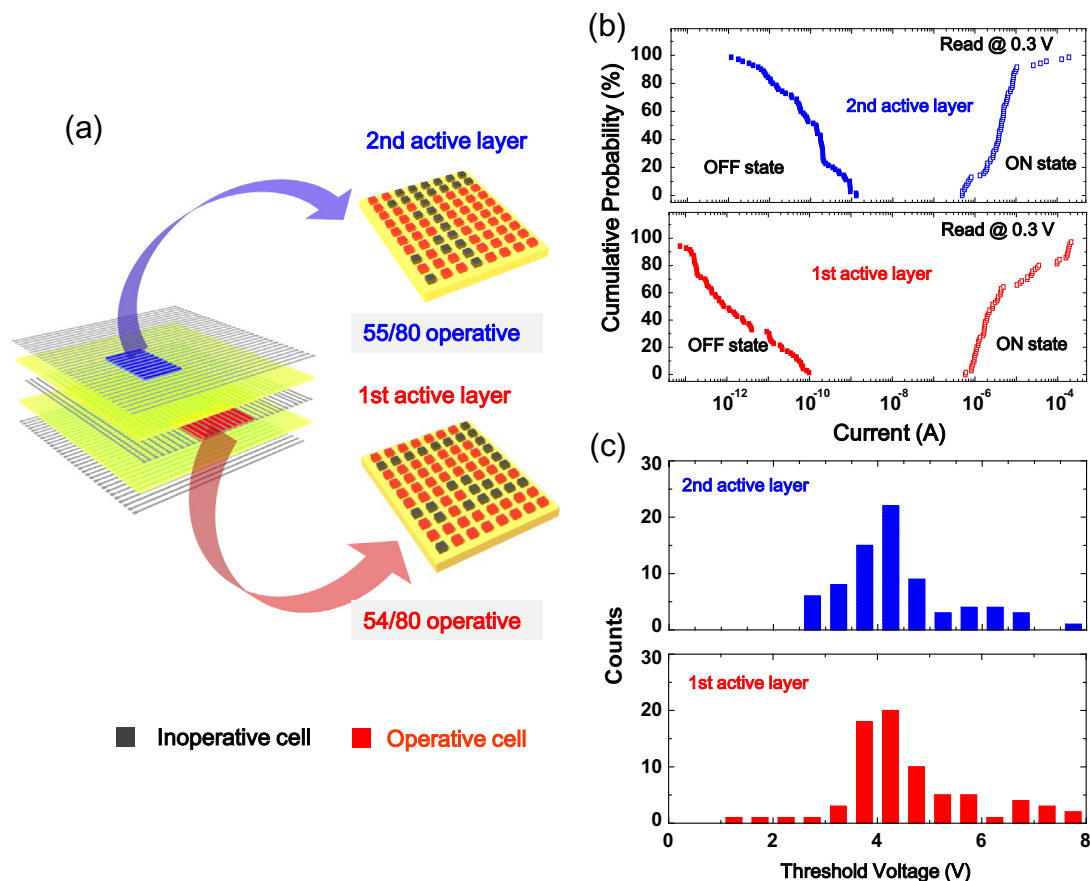
### 3. Results and discussion

Fig. 3a and b present the electrical characteristics of representative cells of the first- and second-layer microscale PI:PCBM memory devices. The electrical measurements were conducted using a semiconductor analyzer system (Model 4200-SCS, Keithley Inc.) at room temperature in a vacuum probe station (JANIS Model ST-500). The insets in these figures show the schematics of the selected memory cells (red and blue marks) to be characterized in the first and second active layers of the vertically stacked microscale organic memory devices. The memory devices in the first and second layers exhibited similar I–V characteristics (Fig. 3a and b). The memory devices were initially in the OFF (i.e., high-resistance) state. The marked first curves in Fig. 3a and b indicate the I–V data that were measured with voltage sweeps from 0 to 8 V and back to 0 V. When the applied voltage increased beyond  $\sim 4$  V, the devices

abruptly turned from the initial OFF state to the ON state (i.e., low resistance state). This voltage at which a transition from the OFF to ON state occurs is called the threshold voltage (also see Fig. 4c). The ON states remained even after the voltage returned to 0 V. The second curve in Fig. 3a and b shows the reset process. When we swept the voltage from 0 to 15 V, the ON state of the device changed to the OFF state after  $\sim 14$  V. When the devices were measured at a low voltage far less than  $\sim 4$  V, the devices maintained the ON or OFF states, indicating the nonvolatile memory feature. From the write-read-erase-read (WRER) cycle pulse measurements, we found that the time required to turn the OFF state to ON state of our memory devices was 50 ms with 5 V pulse (write process), and also 50 ms was required to transit from the ON to OFF state with 13 V pulse (erase process). While we used the read voltage of 0.3 V in the pulse measurement, the ON and OFF currents were consistent with the values observed from the DC-sweeping I–V measurements (Fig. 3a and b). The detailed WRER cycle pulse measurement results are provided in the [supplementary material](#) (Fig. S7). This type of resistive, nonvolatile memory device is called unipolar memory because the ON and OFF states can be controlled by applying voltages in one polarity [29–31]. We plotted the ON/OFF ratio as a function of the applied voltage for the two selected memory devices in the first and second layer.



**Fig. 3.** Representative I–V curves of vertically stacked microscale organic memory devices (a) in the first memory layer and (b) in the second memory layer. (c) ON/OFF ratios as a function of the applied voltage.



**Fig. 4.** (a) A schematic illustration of vertically stacked microscale organic memory devices as double layers of  $32 \times 32$  crossbar arrays. The region in which the memory devices were measured is indicated by a red (first memory layer) or blue rectangle (second memory layer). The right image of (a) summarizes the statistical distribution of the operative memory cells (red) and inoperative memory cells (black). (b) Cumulative probability data for all operative memory cells for each layer. (c) Threshold voltage distribution of operative memory cells for each layer. (For interpretation of the references to color in this figure legend, the reader is referred to the web version of this article.)

The results are shown in Fig. 3c, and the ON/OFF ratio was found to be greater than  $10^4$  in the voltage range less than  $\sim 2$  V.

Fig. 4a illustrates the statistical analysis of the double-layer microscale organic memory devices. The two PI:PCBM organic memory layers (yellow) are sandwiched between pairs of Al electrodes (gray), in which the regions selected to characterize the memory cells are illustrated by a red box for the first layer and a blue box for the second layer. We examined 80 selected cells in each layer (for a total of 160 cells). The right image of Fig. 4a presents the operative memory cells (red) and inoperative memory cells (black). Both layers exhibited a similar device yield of  $\sim 70\%$ , which is comparable value reported for other organic memory devices [26,27,31–34] (see Table S1 in the supplementary material which summarizes the device yield and the statistical distribution of the threshold voltage values reported for the organic memory devices). The detailed I–V data of all measured memory cells in the first and second layers are provided in the supplementary material (Figs. S3–S5). Despite the loss of some memory cells, our vertically stacked microscale organic memory devices operated reasonably well in both layers.

Fig. 4b shows the cumulative probabilities of the switching currents for all operative memory devices in each memory layer. Here, the measured current values were plotted as ON and OFF currents at a read voltage of 0.3 V. Although there are some distributions for both ON and OFF current values, the important point is that the ON and OFF currents are well separated by more than two to three orders of magnitude. Fig. 4c shows the statistical distribution of the threshold voltage (the transition voltage from the OFF state

to the ON state) of the operative memory devices in each memory layer. The threshold voltages values were distributed between 3.5 and 6.5 V for both memory layers. Threshold voltage distribution follows a near Gaussian distribution (see Fig. S6 in the supplementary material). For the first layer, the average threshold voltage was 4.53 V and  $\sigma$  (standard deviation) was 1.27 V. And for the second layer, the average threshold voltage and  $\sigma$  were 4.31 V and 1.03 V, respectively. About 70% memory cells were within  $\sigma$  away from the average threshold voltage value. Because the threshold voltage distributions were found to be similar for both layers, all operative memory cells could be switched ON by uniform parameters.

To examine the memory performance of the vertically stacked microscale organic memory devices, we performed a series of characterizations, such as the DC sweep endurance test and the memory retention test. As shown in Fig. 5a, our memory devices exhibited a reasonable retention property over  $10^4$  s. In this retention test, the current values of the two states (ON and OFF states) were well measured at a read voltage of 0.3 V. Fig. 5b and c shows the results of the DC sweep endurance test for the memory devices in the first and second layers, respectively. DC voltage sweeps were performed 100 times. During the repetitive sweeps, both memory devices maintained ON/OFF ratios above  $10^5$  without showing any significant electrical degradation. This reliable electrical performance highlights the potential for highly integrated, microscale, organic memory-device applications. This result demonstrated that orthogonal photolithography used for the vertically stacked microscale organic memory devices did not damage the underlying

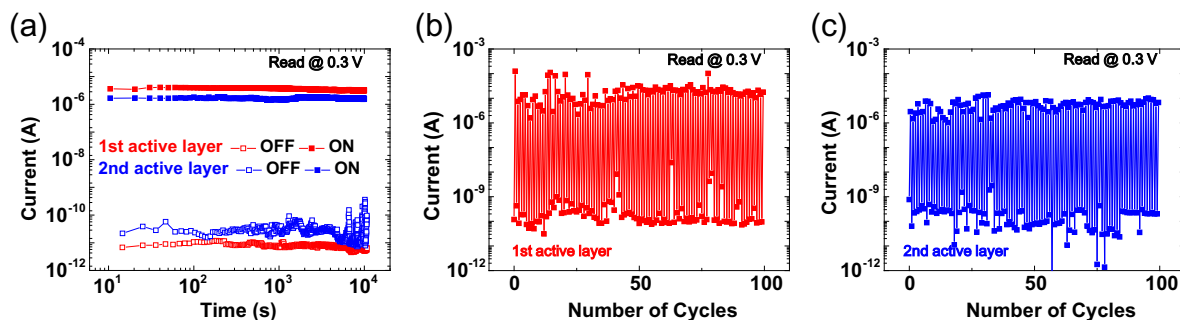


Fig. 5. (a) Retention time characteristics and (b) DC sweep endurance test results of the vertically stacked microscale organic memory devices.

organic layers. Therefore, our study can be used to produce highly integrated microscale organic memory devices with high memory performance.

#### 4. Conclusions

In summary, we fabricated vertically stacked microscale PI:PCBM organic resistive nonvolatile memory devices. The devices were fabricated as double layers of  $32 \times 32$  crossbar arrays (total of 2048 memory cells) with an individual memory-cell size of  $7 \times 7 \mu\text{m}^2$ , which was possible using orthogonal photolithography with a special fluorinated photoresist and development solvent. The fabricated vertically stacked microscale organic memory devices exhibited stable electrical characteristics, and the operative memory devices in the first and second layers had similar memory operation properties, such as ON/OFF ratio, statistical distribution, and threshold voltages. We demonstrated reliable memory performances of our vertically stacked microscale organic memory devices in terms of endurance cycles and retention time. Our study might foster more practical device applications toward the three-dimensional integration of microscale organic electronic devices.

#### Acknowledgements

The authors acknowledge the financial support from the National Creative Research Laboratory program (Grant no. 2012026372) and the National Core Research Center (Grant no. 2008-0062606) through the National Research Foundation of Korea (NRF) funded by the Korean Ministry of Science, ICT & Future Planning. S.H. acknowledges the support from NRF grant No. 2013M3C8A3078813. J.-K.L. thanks the financial support from the Fundamental R&D Program for Core Technology of Materials (Grant no. 10041220) funded by the Korean Ministry of Trade, Industry & Energy.

#### Appendix A. Supplementary data

Supplementary data associated with this article can be found, in the online version, at <http://dx.doi.org/10.1016/j.orgel.2015.03.023>.

#### References

[1] S.R. Forrest, *Nature* 428 (2004) 911.

- [2] H.T. Yi, M.M. Payne, J.E. Anthony, V. Podzorov, *Nat. Commun.* 3 (2012) 1259.
- [3] L.S. Zhou, A. Wanga, S.C. Wu, J. Sun, S. Park, T.N. Jackson, *Appl. Phys. Lett.* 88 (2006) 083502.
- [4] Y.-Y. Noh, N. Zhao, M. Caironi, H. Sirringhaus, *Nat. Nanotechnol.* 2 (2007) 784.
- [5] J.C. Scott, L.D. Bozano, *Adv. Mater.* 19 (2007) 1452.
- [6] R.R. Sondergaard, M. Hoesel, F.C. Krebs, *J. Polym. Sci. Polym. Phys.* 51 (2013) 16.
- [7] R.J. Tseng, J. Huang, J. Ouyang, R.B. Kaner, Y. Yang, *Nano Lett.* 5 (2005) 1077.
- [8] T. Lei, Y. Cao, Y. Fan, C.J. Liu, S.C. Yuan, J. Pei, *J. Am. Chem. Soc.* 133 (2011) 16.
- [9] T.H. Han, Y. Lee, M.R. Choi, S.H. Woo, S.H. Bae, B.H. Hong, J.H. Ahn, T.-W. Lee, *Nat. Photonics* 6 (2012) 105.
- [10] C. Min, J. Li, G. Veronis, J.Y. Lee, S. Fan, P. Peumans, *Appl. Phys. Lett.* 96 (2010) 133302.
- [11] R. Fitzner, E.M. Osteritz, A. Mishra, G. Schulz, E. Reinold, M. Weil, C. Korner, H. Ziehlke, C. Elschner, H. Ziehlke, C. Elschner, K. Leo, M. Riede, M. Pfeiffer, C. Uhrich, P. Bauerle, *J. Am. Chem. Soc.* 134 (2012) 27.
- [12] S.J. Kang, I. Bae, Y.J. Park, T.H. Park, J. Sung, S.C. Yoon, K.H. Kim, D.H. Choi, C. Park, *Adv. Funct. Mater.* 19 (2009) 1609.
- [13] B. Cho, S. Song, Y. Ji, T.-W. Kim, T. Lee, *Adv. Funct. Mater.* 21 (2011) 2806.
- [14] S. Song, J. Jang, Y. Ji, S. Park, T.-W. Kim, Y. Song, M.H. Yoon, H.C. Ko, G.Y. Jung, T. Lee, *Org. Electron.* 14 (2013) 2087.
- [15] T. Lee, Y. Chen, *MRS Bull.* 37 (2012) 144.
- [16] B. Cho, S. Song, Y. Ji, H.G. Choi, H.C. Ko, J.S. Lee, G.Y. Jung, T. Lee, *IEEE Electron Devices Lett.* 34 (2013) 1.
- [17] M.L. Chabiny, A. Salleo, *Chem. Mater.* 16 (2004) 4509.
- [18] H. Klauk, U. Zschieschang, J. Pflaum, M. Halik, *Nature* 445 (2007) 745.
- [19] S. Ju, J. Li, J. Liu, P.C. Chen, Y.G. Ha, F. Ishikawa, H. Chang, C. Zhou, A. Facchetti, D.B. Janes, T.J. Marks, *Nano Lett.* 8 (2008) 997.
- [20] J.K. Lee, M. Chatzchristidi, A.A. Zakhidov, P.G. Taylor, J.A. DeFranco, H.S. Hwang, H.H. Fong, A.B. Holmes, G.G. Malliaras, C.K. Ober, *J. Am. Chem. Soc.* 130 (2008) 11564.
- [21] A.A. Zakhidov, H. Fong, J.A. DeFranco, J.-K. Lee, P.G. Taylor, C.K. Ober, G.G. Malliaras, M. He, M.G. Kane, *Appl. Phys. Lett.* 99 (2011) 183308.
- [22] J. Jang, Y. Song, H. Oh, D. Yoo, D. Kim, H. Lee, S. Hong, J.K. Lee, T. Lee, *Appl. Phys. Lett.* 104 (2014) 053301.
- [23] J. Jang, Y. Song, D. Yoo, T.Y. Kim, S.H. Jung, S. Hong, J.K. Lee, T. Lee, *Org. Electron.* 15 (2014) 2822.
- [24] Y. Song, J. Jang, D. Yoo, S.-H. Jung, S. Hong, J.-K. Lee, T. Lee, *Org. Electron.* 17 (2015) 192.
- [25] C. Kugeler, M. Meier, R. Rosezin, S. Gilles, R. Waser, *Solid State Electron.* 53 (2009) 1287.
- [26] S. Song, B. Cho, T.-W. Kim, Y. Ji, M. Jo, G. Wang, M. Choe, Y.H. Kahng, H. Hwang, T. Lee, *Adv. Mater.* 22 (2010) 5048.
- [27] Y. Ji, D.F. Zeiger, D.S. Lee, H. Choi, A.K.-Y. Jen, H.C. Ko, T.-W. Kim, *Nat. Commun.* 4 (2013) 2707.
- [28] B. Cho, K.H. Nam, S. Song, Y. Ji, G.Y. Jung, T. Lee, *Curr. Appl. Phys.* 12 (2012) 940.
- [29] F. Verbakel, S.C.J. Meskers, R.A.J. Janssen, H.L. Gomes, M. Colle, M. Buchel, D.M. Leeuw, *Appl. Phys. Lett.* 91 (2007) 192103.
- [30] B. Cho, T.-W. Kim, M. Choe, G. Wang, S. Song, T. Lee, *Org. Electron.* 10 (2009) 473.
- [31] J.J. Kim, B. Cho, K.S. Kim, T. Lee, G.Y. Jung, *Adv. Mater.* 23 (2011) 2104.
- [32] C. Wu, F. Li, Y. Zhang, T. Guo, T. Chen, *Appl. Phys. Lett.* 99 (2011) 042108.
- [33] S.G. Hamm, N.-G. Kang, W. Kwon, K. Kim, Y.-G. Ko, S. Ahn, B.-G. Kang, T. Chang, J.-S. Lee, M. Ree, *Adv. Mater.* 24 (2012) 1062.
- [34] N.-G. Kang, B. Cho, B.-G. Kang, S. Song, T. Lee, J.-S. Lee, *Adv. Mater.* 24 (2012) 385.